ADVANCED FUNCTIONAL MATERIALS
www.afm-journal.de

Materials Views
www.MaterialsViews.com

# The Role of Sulfur in Solution-Processed $Cu_2ZnSn(S,Se)_4$ and its Effect on Defect Properties

*Hsin-Sheng Duan, Wenbing Yang, Brion Bob, Chia-Jung Hsu, Bao Lei, and Yang Yang**

**Understanding the electrically active defects in kesterite $Cu_2ZnSn(S,Se)_4$(CZTSSe) is critical for the continued development of solar cells based on this material, but challenging due to the complex nature of this polycrystalline multinary material. A comparative study of CZTSSe alloys with three different bandgaps, made by introducing different fractions of sulfur during the annealing process, is presented. Using admittance spectroscopy, drive level capacitance profiling, and capacitance-voltage profiling, the dominant defect energy level present in the low sulfur content device is determined to be 0.134 eV above the valence band maximum, with a bulk defect density of $8 \times 10^{14}$ cm$^{-3}$, while the high sulfur content device shows a deeper defect energy level of 0.183 eV and a higher bulk defect density, $8.2 \times 10^{15}$ cm$^{-3}$. These findings are consistent with the current density–voltage characteristics of the resulting solar cells and their external quantum efficiency. It suggests that as the sulfur content increases, the bandgap of the absorber is enlarged, leading to an increasing open-circuit voltage ($V_{oc}$), that is accompanied by stronger recombination due to the higher defect density of the sulfur-rich absorber. This is reflected in large $V_{oc}$ deficit and poor carrier collection of the high sulfur content device.**

## 1. Introduction

Kesterite, $Cu_2ZnSn(S,Se)_4$ (CZTSSe), photovoltaics are considered a potential alternative to traditional chalcogenide-based thin film solar cells (e.g., $Cu(In,Ga)(S,Se)_2$ and CdTe) because of its earth-abundant and non-toxic constituents. Since 2010, high efficiency (>8%) $Cu_2ZnSn(S,Se)_4$ photovoltaics have been demonstrated successfully via various approaches. Several reports include an 11.1% device made by spin-coating particle-containing hydrazine precursor slurries and annealing on a hot plate,[1–3] an 8.1% device made by using molecular level homogeneous hydrazine precursor solution,[4] an 8.4% device made by annealing colloidal nanocrystals in selenium vapor,[5] and with the use of the coevaporation technique a 9.15%[6] and an 8.4%[7] device were reported. While these early-stage developments show a promising future for kesterite photovoltaics, it is also important to understand its defect physics and recombination mechanisms.[8] This understanding is urgently needed for further improvement of the cell characteristics to a level comparable with $Cu(In,Ga)(S,Se)_2$(CIGS) and CdTe.

The majority of previous reports[1–7,9–11] have shown that the highest-efficiency kesterite solar cells are made of CZTSSe alloys with high selenium (Se) content rather than high sulfur (S) content, despite the fact that the sulfur-rich compound has a more optimal bandgap, 1.4 eV, according to theoretical calculations.[12] In the case of $Cu(In_xGa_{1-x})Se_2$, high gallium (Ga) concentration is not beneficial for the device performance since CuGaSe2 is difficult to be doped as n-type,[13,14] resulting in the absence of an n-type inverted layer in CuGaSe2 absorbers which facilitates carrier extraction. With the use of the first-principle calculations and Density Functional Theory, Chen et al.[15] reported that CZTSSe alloys with high Se content are more easily converted to n-type semiconductor and thus CZTSSe solar cells with high Se content are expected to have better carrier collection efficiency than CZTS. Besides, it was reported that the self p-type doping in kesterite are mainly related to $Cu_{Zn}$ antisite defects and $V_{Cu}$ (Cu vacancies).[16] The energy level of $Cu_{Zn}$ antisites becomes shallower (closer to the valence band) as sulfur concentration decreases in CZTSSe alloys because in CZTS, the stronger hybridization between the sulfur 3p and copper 3d orbitals brings the valence band lower. Based on these simulated results, high efficiency CZTSe (low S content) devices should be achievable because of more facile n-type and p-type doping than CZTS (high S content). However, attempts to experimentally investigate defect properties in the kesterite family[17,18] have not yet reached the level of maturity of the well-established field of defects physics in chalcopyrite-based devices.[19–22]

In this paper, we report a comparative study of solution-processed kesterite CZTSSe cells with three different bandgaps (resulting from three different Se and S concentrations in alloys). We aim at correlating the electrical defect levels of CZTSSe, observed through admittance spectroscopy and charge density profiling, with the cells' characteristics deduced from current density-voltage and quantum efficiency measurements. Based on the experiment results, we have found that changes in

H.-S. Duan, W. Yang, B. Bob, C.-J. Hsu,
Dr. B. Lei, Prof. Y. Yang
Department of Materials Science and Engineering and California NanoSystem Institute
University of California Los Angeles
Los Angeles, CA 90095, USA
E-mail: yangy@ucla.edu

DOI: 10.1002/adfm.201201732

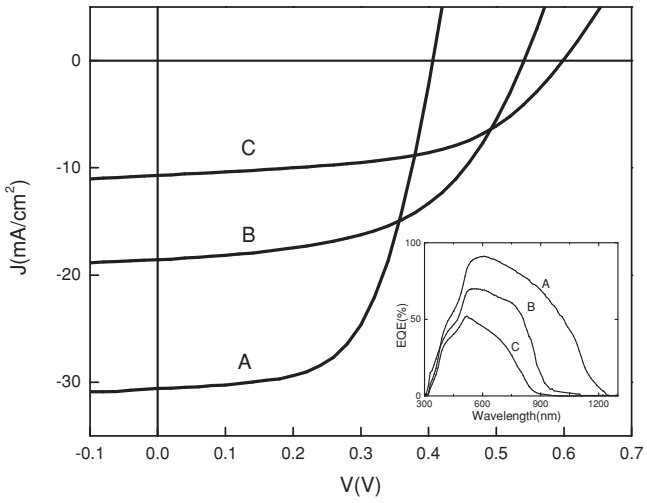


**Figure 1.** Light *J–V* data of CZTSSe devices with various sulfur content. Low sulfur content device (A) shows the highest efficiency ≈7.4%. Inset: corresponding external quantum efficiency.

the S and Se ratio significantly alters both the energy level and concentration of the dominant defects, and ultimately produces the poor carrier collection efficiency and larger losses of open circuit voltage as a result of the increasing numbers of observed recombination centers.

## 2. Results and Discussion

### 2.1. Current–Voltage Characteristics

**Figure 1** shows the illuminated current density–voltage (*J–V*) characteristic curves for devices with different amounts of selenium and sulfur, with the corresponding external quantum efficiency (EQE) curves shown in the inset. The cell parameters deduced from *J–V* measurements, as well as the bandgap deduced from the long-wavelength cutoff of the EQE[23] are summarized in **Table 1**. The devices A, B, and C correspond to three different S contents of [S]/([S]+[Se]) ≈ 0.35, 0.8 and 1, respectively. CZTSSe films were deposited through hydrazine solution processing. X-ray diffraction and Raman data indicate the presence of only the kesterite phase in the films and are discussed in detail in a separate publication.[4]

**Table 1.** Device parameters for CZTSSe cells at room temperature with various [S]/([S]+[Se]) ratio.

| Device | Eff [%] | $V_{oc}$ [V] | $E_g$ [eV] | $E_g$-$qV_{oc}$ [eV] | $J_{sc}$ [mA/cm$^2$] | FF [%] |
|---|---|---|---|---|---|---|
| Sample A | 7.4 | 0.406 | 1.15 | 0.74 | 30.5 | 59.55 |
| Sample B | 5.3 | 0.541 | 1.35 | 0.81 | 18.5 | 53.57 |
| Sample C | 3.5 | 0.599 | 1.5 | 0.90 | 10.7 | 54.28 |

The device with high sulfur content has a higher open-circuit voltage (≈0.6 V), consistent with its large bandgap (≈1.5 eV). The device with low sulfur content has relatively small open-circuit voltage (0.406 V) but has much larger short-circuit current density ($J_{sc}$), mainly due to improved carrier collection at longer wavelengths. Among the three devices, low sulfur content device (sample A) gives the highest power conversion efficiency of 7.4%. In EQE data measured at 0 V (Figure 1b), the high sulfur content device (sample C) has a lower peak value than the others. This reveals that the S concentration in the alloy not only changes the bandgap but also gives rise to stronger recombination losses.[24,25]

### 2.2. Admittance Spectroscopy

Admittance spectroscopy (AS) measurements, which are commonly used to estimate the energy level of defects inside the band gap, were taken on each of the three types of samples. Capacitance-frequency (CF) scans taken in the temperature range 160 K to 300 K are shown in **Figure 2**. CF scans were measured in the dark from $10^2$ to $10^6$ Hz. An AC voltage of 30 mV was used and DC bias was kept at zero during the measurement.

Using the model implied by the work of Kimerling,[26] the capacitance at high frequency represents the response of the free carrier density, while the capacitance at low frequency represents the response of the sum of free carriers and deep traps. In Figure 2c, the capacitance of the device with high sulfur content shows a larger variation as a function of frequency, while the capacitance of the devices with low sulfur content show small changes between high and low frequencies (Figure 2a). The significant frequency dependence of the capacitance in the high sulfur content device indicates larger trap densities in the absorber. A similar trend of has been reported recently

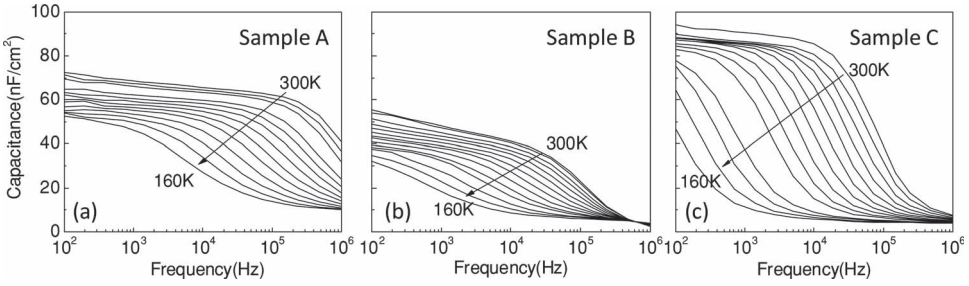


**Figure 2.** Admittance spectra of devices with various sulfur content, measured at temperature between 160 K and 300 K with a step of 10 K. The *y*-axes of the three plots have been scaled to be the same.

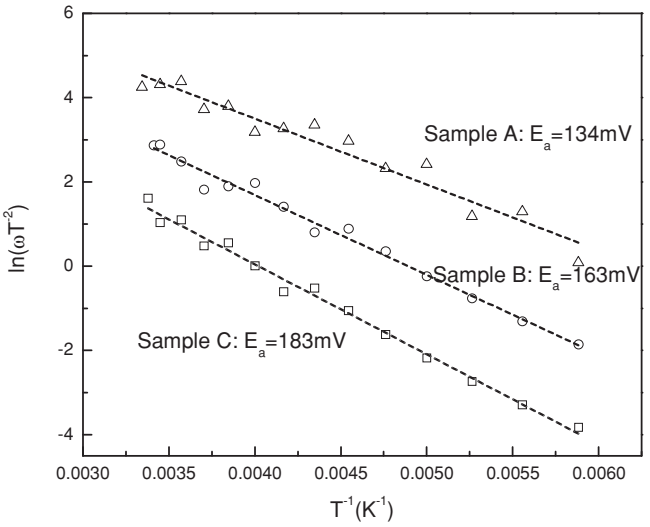


**Figure 3.** Arrhenius plot of the inflection frequencies determined from the derivative of the admittance spectra.

for devices with bandgaps falling in the range of 1.0 to 1.5 eV.[18] In Figure 2b,c, it is visible that the capacitance data converges at high frequency and low temperature, where it is likely determined by the geometric capacitance of the devices due to carrier freeze-out.[27]

**Figure 3** shows the Arrhenius plot for the inflection points in the three admittance spectra in Figure 2. The step frequency $\omega_0$ (or inflection point frequency) for each AS curve is determined by using the angular frequency point at the maximum of the $\omega dC/d\omega$ plot. The fitting of the Arrhenius plot is according to the equation:[20]

$$\omega_0 = 2\pi\nu_0 T^2 \exp\left(\frac{-E_a}{kT}\right) \quad (1)$$

where $\omega_0$ is the step frequency, $E_a$ is the energetic depth of the defect relative to the corresponding band edge, and $\nu_0$ is the pre-exponential factor comprising all temperature-independent terms, such as defect capture cross section for holes $\sigma_p$, effective density of states in the valence band $N_V$, and thermal velocity $\upsilon_{th}$.

In this case, the activation energy $E_a$ determined by the Arrhenius plot is approximately the energy difference between defect level and valence band edge. Assuming that their energy levels are within a small range, the $E_a$ value deduced from the Arrhenius plot can also represent the average value of activation energies of a band of defects in the bandgap. The activation energy $E_a$ is around 0.134 eV, 0.163 eV and 0.183 eV for devices A, B and C (from low to high sulfur content), respectively. In addition, we calculated the pre-exponential factors, which is around the order of $10^3$ for all devices.

A general increase of activation energy with increasing sulfur fraction in the absorber is clearly visible in the admittance spectroscopy data. The change of defect activation energy in three samples is possibly related to the shifts of the valence band maximum resulting from the differing sulfur concentrations in the CZTSSe absorber. As the sulfur content increases in CZTSSe alloys, the valence band moves down, potentially yielding defects with higher ionization energies.[15] A larger value of $E_a$ is generally an indicator of a slower hole emission rate, corresponding to the lower transition frequency in the AS curves, and thus it is more likely that defects with larger activation energies tend to act as more effective recombination centers. The defect response in the high sulfur content device occurred at a higher energy (0.183 eV) than in the low sulfur content device (0.134 eV). Thus, the low sulfur content device can be expected to experience relatively lower recombination rates than the high sulfur content one. This observation can also be correlated with external quantum efficiency (Figure 1b). The high sulfur content device exhibited much lower quantum efficiency, likely as a result of significant recombination losses due to increased defect activity.

Defect density spectra resulting from CF scans at each temperature (Figure 2) are superimposed in **Figure 4**. For each sample, the calculation of the rescaling factor of the y-axis, including the band-bending and built-in voltage, uses typical values reported in literature,[28] and the conversion of the *x*-axis from frequency to energy is achieved following Equation (1). The dashed line is the Gaussian fit to the respective defect energy level, as described in the work of Walter et al.[20] The integrated defect density of the low sulfur content device is $4.96 \times 10^{15}$ cm$^{-3}$, which is relatively smaller than the value of the high sulfur content device, $1.14 \times 10^{16}$ cm$^{-3}$. We also noticed that these integrated defect densities are roughly proportional to the difference between the largest capacitance value and smallest capacitance value in CF scans.

In each of the three cases, the calculated activation energies are between 0.1 and 0.2 eV, so this defect level could potentially

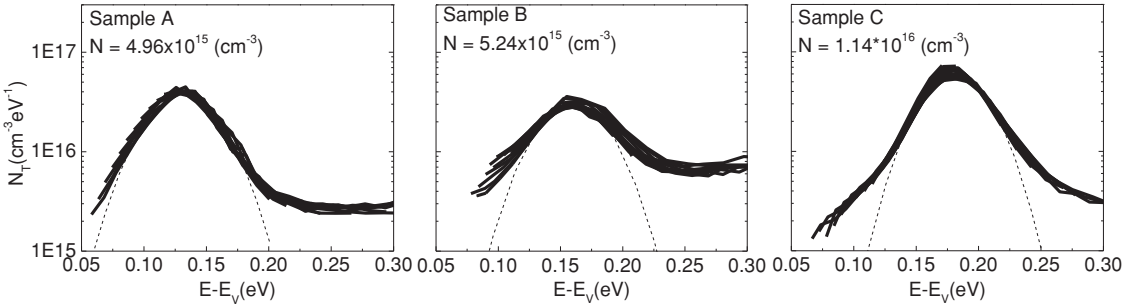


**Figure 4.** Defect spectra derived from admittance spectra. The *y*-axis of three plots have been scaled to be the same.

be ascribed to a structure similar to the N1 trap level commonly observed in CIGS.[29] Similar defect levels in kesterite were also found by other groups.[17,18] Note that the defect state at 0.3 eV above the valence band, known as the N2 defect in CIGS,[29] was not found in our measurement. The origin of the N1 defect level remains unclear, but in chalcogenide photovoltaics it has been assigned to several possible sources, such as $(In,Ga)_{Cu}$ defects at the CIGS surface,[30] defects at the CIGS/CdS interface,[29] bulk defects inside the CIGS absorber,[31] defects at the CIGS/Mo back contact,[32] or surface anion vacancies $V_{Se}$ that involve interfacial donors.[33,34] In this work, a possible source of the observed acceptor level is the $Cu_{Zn}$ antisite, which has the lowest formation energy and is located at 0.12 eV above the valence band, according to first principle calculations.

Copper vacancies, commonly assigned as the primary p-type dopants in CIGS,[35] are predicted to be a relatively shallow defect at 0.02 eV above the valence band in kesterite, but with higher formation energies than $Cu_{Zn}$ antisite.[16] However, this defect energy level was not observed in AS measurements. It is controversial whether or not copper-on-zinc antisites or copper vacancies are the dominant acceptors in kesterite.[8,36] Several photoluminescence (PL) studies of defects in kesterite alloys showed donor-acceptor (DA) pair transitions at low temperatures, indicative of a shallow acceptor level around 30 meV or less, in Cu-rich samples.[37,38] A recent study films with metallic ratios of [Cu]/([Zn] + [Sn]) = 0.9 and [Zn]/[Sn] = 1.3, observed an acceptor level in the range of 29–40 meV above the valence band via the fitting of PL intensity at various temperatures.[39] Meanwhile, broad emission spectra were detected in both photoluminescence and cathodoluminescence in Cu-poor and Zn-rich films, suggesting localized potential fluctuations in the conduction band minimum and valence band maximum.[36,39] The fluctuation of energy levels was estimated to a value of 172 ± 2 meV. With regard to the huge conduction and valence band fluctuation, it is possible that the ionization energy of acceptors deduced from the PL intensity-temperature plot is underestimated, and thus, the exact defect energy level seen in luminescence is comparable with the AS results.

### 2.3. Drive-Level Capacitance Profiling

Though traditional capacitance profiling data can provide the spatial defect density as deduced from capacitance-voltage (CV) scans, it is unable to distinguish between the bulk and interface defects, since both types of defects respond to this type of measurement. In order to identify different types of defects in the film (bulk defects, interface defects, and free carriers), drive-level capacitance profiling (DLCP) measurements were employed by using the technique of Heath et al.,[21] supplemented with CV profiling measurement (not shown here). Compared to CV measurements, DLCP gives a more accurate assessment of the free carrier density in the film, while CV measurements are more sensitive to interface states which commonly exist in chalcopyrite-based cells. In the method that Heath et al. developed, the contribution of the interface states can be extracted by a subtraction of DLCP defect density from CV defect density.[31] These will be discussed in detail later.

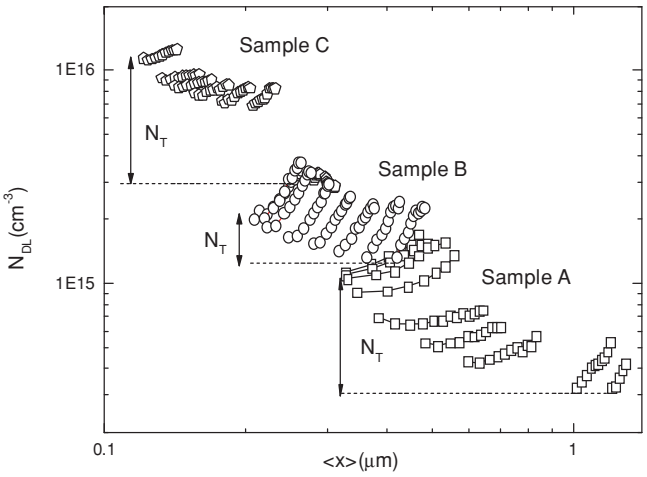


**Figure 5.** Deep-level response of various sulfur content devices at different temperatures. The measurement frequency was 11 kHz, the dc bias range was 0 V to –0.5 V, and the temperature range was 160 K to 300 K.

DLCP measurements were performed with DC bias from –0.5 to 0 V with the AC amplitude varying from 0.01 V to 0.1 V, and temperature range from 160 K to 300 K. The measurement frequency of 11 kHz was selected. We estimated that, in the low sulfur device (sample A), DLCP response at 160 K corresponds to $E_a$ (activation energy) = 0.12 eV while DLCP response at 300 K corresponds to $E_a$ = 0.25 eV, with the other devices exhibiting comparable activation energy measurement ranges. AS for all three devices indicate defects with characteristics energy between 0.1–0.2 eV; thus our range of profiling spans the energy response of these defects at all three absorber compositions. The charge density was determined by the relevant relation described in literature.[21] The resulting charge density, $N_{DL}$, is shown in **Figure 5** (the horizontal axis is $\langle x \rangle = \varepsilon A/C_0$, the average location of charges response to AC signal, where $C_0$ is from a quadratic fit of measured capacitance $dQ/dV$, $\varepsilon$ is the permittivity of the CZTSSe absorber layer,[40] and $A$ is the device area).

Here, we assumed that the entire depletion region is mainly in the CZTSSe absorber layer because of the high n-type doping concentration of the CdS layer. Therefore $N_{DL}$, measured by DLCP, represents the charge density of the CZTSSe layer. At high temperatures, DLCP is capable of observing the response from free carrier and deep defects, but at sufficiently low temperatures only free carriers contribute to the DLCP signal. Thus, the subtraction of the low temperature $N_{DL}$ value from the high temperature $N_{DL}$ value is closely correlated to the defect density in the absorber.[21] The $N_{DL}$ points at $V_{dc} = 0$ were chosen to estimate the defect density (the defect density is labeled as $N_T$ in Figure 5). The estimated values for each condition are listed in **Table 2**. The high sulfur content device possesses a larger bulk defect density than the low sulfur content one. This trend is consistent with the AS data, where the high sulfur content device exhibited a larger capacitance variation, as a function of frequency.

Secondly, by applying the subtraction of the low temperature $N_{DL}$ from the high temperature $N_{DL}$, the high sulfur content

**Table 2.** Summary of the results derived from DLCP measurements.

| Device | Free carriers density [$cm^{-3}$] | Trap density [$cm^{-3}$] | Interface state response [relative values] |
|---|---|---|---|
| Sample A | $3.22 \times 10^{14}$ | $8 \times 10^{14}$ | $1.17 \times 10^{16}$ |
| Sample B | $1.33 \times 10^{15}$ | $9 \times 10^{14}$ | $1.07 \times 10^{16}$ |
| Sample C | $3.15 \times 10^{15}$ | $8.22 \times 10^{15}$ | $1.81 \times 10^{16}$ |

device has approximately an order of magnitude larger free carrier concentration than the low sulfur content device. The free carrier density derived from DLCP generally corresponds to the density of fully ionized dopants,[21] indicating the dependence of doping concentration on sulfur content as seen in Table 2. It is known that the semiconductors with high doping concentration have greater recombination, resulting in shorter minority carrier lifetimes as well as shorter diffusion lengths. Thus, the dependence of doping concentration on sulfur content is consistent with previous reports showing that CZTSe (almost no sulfur content in the device) has longer carrier lifetime (10 ns) than CZTSSe (low sulfur content, 3 ns).[2] This finding also explains the high recombination losses in the high sulfur content device as a result of its high doping concentration. While the structural origin of the high doping concentration on sulfur content is inconclusive at this point, the changes in carrier concentration observed here are possibly related to varying levels of compensation from donor defects, such as anion vacancies ($V_S$ or $V_{Se}$) that may be dependent on the sulfur and selenium content of the absorber material.[41,42] A more detailed understanding of this behavior is currently under investigation.

Thirdly, the defect concentration is expected to be a major determinant of open circuit voltage ($V_{oc}$), and the voltage shortfall, $E_g$–$qV_{oc}$, and defect density can be correlated in the relation:[43]

$$E_g - q\,V_{oc} \propto A \ln N \tag{2}$$

where $E_g$ is the bandgap energy, $q$ denotes the elementary charge, $A$ is the diode ideal factor and $N$ is the concentration of rembination centers in the bulk of the CZTSSe film.[43] The defect density measured from AS (Figure 2) and from DLCP (Figure 5) both correlate with the voltage shortfall shown in Table 1. As the voltage deficit increases, so does defect density detected by AS and DLCP. This correlation shows that the open cuicuit voltage losses result from high bulk defect concentations in absorber materials that have higher sulfur content.

As mentioned earlier, the effect of interface defects can be relatively quantified based on the subtraction of DLCP-evaluated charge density at room temperature from CV-evaluated charge density at room temperature,[31] where the points at zero DC bias were used in the calculation. While the resulting interface state response in all three samples is on the same order of magnitude, the high sulfur content device exhibits a relatively higher interface defect density, suggesting that the interfacial defects are related the open circuit voltage losses seen in the device performance section of this study. Furthermore, as seen in the plot of $V_{oc}$ versus temperature in the recent reports,[1,25] the deduced value of activation energy of recombination suggested that the deficiency in $V_{oc}$ is strongly influenced by interface recombination, possibly at the absorber/buffer interface.[44] By contrast, it has been demonstrated that in CIGS space charge recombination (SCR) is dominant. Thus, it should be expected that the interface state response of CZTSSe is much stronger than the response of CIGS. However, enhanced interface defect response is not evident in CZTSSe cells, compared to CIGS data in the literature.[45]

## 3. Conclusions

By employing admittance spectroscopy and carrier density profiling measurements at various temperatures, we have observed the influence of sulfur content in CZTSSe alloys on defect activation energy, defect density, and photovoltaic performance. The high sulfur content device showed higher defect energy level (0.183 eV) as well as high bulk defect density ($8.2 \times 10^{15}$ $cm^{-3}$), and this behavior of defects leads to the strong recombination losses as indicated by low external quantum efficiency values and a large $V_{oc}$ deficit. In contrast, the low sulfur content absorber showed the best performance (7.4%) and highest external quantum efficiency as a result of the relatively low activation energy (0.134 eV) and the low bulk defect density ($8 \times 10^{14}$ $cm^{-3}$). Overall, when enlarging the bandgap of the absorber by increasing its sulfur content, the open-circuit voltage increases, but overall device efficiency is reduced. These findings provide a better understanding of defect properties in kesterite alloys, which are critical for the control of recombination processes, doping, and junction formation in solar cells fabricated from this material.

## 4. Experimental Section

*Device Fabrication*: CZTSSe hydrazine-based precursor solutions were prepared in a nitrogen filled glove box. Cu-constituent and Sn-constituent solutions were prepared following the procedures describe elsewhere.[46,47] For Zn-constituent solution, the hydrazinocarboxylic acid ($NH_2NHCOOH$) was used to fully dissolve zinc powder in hydrazine. Final CZTS precursor solutions were prepared by mixing all constituent solutions with a final ratio of Zn/Sn = 1.2, Cu/(Zn+Sn) = 0.8. Detailed procedures of CZTSSe precursor solution and film preparation can be found in a separation publication.[4]

CZTSSe films were then deposited by spin-coating the precursor solution on molybdenum coated soda lime glass substrates. To prepare the absorber layers with different bandgaps, various amount of chalcogen vapor, including pure selenium vapor, pure sulfur vapor and mixed selenium and sulfur vapor, were supplied during the annealing at 500 °C on a ceramic hot plate. A CdS buffer layer was completed via a standard chemical bath deposition,[22] and ZnO and ITO were deposited on top with the RF sputtering system, giving a standard device structure: glass/Mo/CZTSSe/CdS/ZnO/ITO with nominal area 0.1 $cm^2$, determined by mechanically scribing all layers aside from the molybdenum back contact.

*Device Characterization*: The *J–V* characteristics of the photovoltaic devices were measured using a Keithley 2400 source meter. Illumination was provided by a Newport Oriel solar simulator (Model 91191-1000) with an AM 1.5G filter (Model 81088). The light intensity was stabilized at 100 mW/$cm^2$ using a Newport Oriel 68945 light intensity controller. The EQE was measured using a system designed by EnliTech. The capacitance of the photovoltaic device was measured using a Hewlett-Packard 4284A LCR Meter. Temperature-dependent measurements were

carried out using a Linkam temperature-controlled stage equipped with liquid nitrogen cooling. The temperature was monitored by a calibrated platinum sensor embedded close to the surface of the stage.

## Acknowledgements

The authors would like to thank Steve Hawks for the assistance on temperature-dependent measurement and Simson Chiu for proofreading the manuscript.

Received: June 26, 2012
Revised: September 21, 2012
Published online: October 16, 2012

[1] D. A. R. Barkhouse, O. Gunawan, T. Gokmen, T. K. Todorov, D. B. Mitzi, *Prog. Photovoltaics* **2012**, *20*, 6.
[2] S. Bag, O. Gunawan, T. Gokmen, Y. Zhu, T. K. Todorov, D. B. Mitzi, *Energy Environ. Sci.* **2012**, *5*, 7060.
[3] T. K. Todorov, J. Tang, S. Bag, O. Gunawan, T. Gokmen, Y. Zhu, D. B. Mitzi, *Adv. Energy Mater.* **2012**, DOI: 10.1002/aenm.201200348.
[4] W. Yang, H.-S. Duan, B. Bob, H. Zhou, B. Lei, C. Chung, S. Li, W. W. Hou, Y. Yang, *Adv. Mater.* **2012**, DOI: 10.1002/adma.201201785.
[5] Q. Guo, G. M. Ford, H. W. Hillhouse, R. Agrawal, presented at *37th IEEE Photovoltaics Specialists Conference (PVSC 37), Seattle, WA, June 19-24,* **2011**.
[6] I. Repins, C. Beall, N. Vora, C. DeHart, D. Kuciauskas, P. Dippo, B. To, J. Mann, W.-C. Hsu, A. Goodrich, R. Noufi, *Sol. Energy Mater. Sol. Cells* **2012**, *101*, 154.
[7] B. Shin, O. Gunawan, Y. Zhu, N. A. Bojarczuk, S. J. Chey, S. Guha, *Prog. Photovoltaics* **2011**, 8.
[8] S. Siebentritt, S. Schorr, *Prog. Photovoltaics* **2012**, *20*, 512.
[9] T. K. Todorov, K. B. Reuter, D. B. Mitzi, *Adv. Mater.* **2010**, *22*, E156.
[10] T. Todorov, O. Gunawan, S. J. Chey, T. G. de Monsabert, A. Prabhakar, D. B. Mitzi, *Thin Solid Films* **2011**, *519*, 7378.
[11] S. Ahmed, K. B. Reuter, O. Gunawan, L. Guo, L. T. Romankiw, H. Deligianni, *Adv Energy Mater.* **2012**, *2*, 253.
[12] M. Contreras, L. Mansfield, B. Egaas, J. Li, M. Romero, R. Noufi, E. Rudiger-Voigt, W. Mannstadt, *Prog. Photovoltaics* DOI: 10.1002/pip.2244.
[13] C. Persson, Y.-J. Zhao, S. Lany, A. Zunger, *Phys. Rev. B* **2005**, *72*, 035211.
[14] S. Wei, S. Zhang, *J. Phys. Chem. Solids* **2005**, *66*, 1994.
[15] S. Chen, A. Walsh, J.-H. Yang, X. Gong, L. Sun, P.-X. Yang, J.-H. Chu, S.-H. Wei, *Phys. Rev. B* **2011**, *83*, 125201.
[16] S. Chen, J. Yang, X. Gong, A. Walsh, *Phys. Rev. B* **2010**, *81*, 35.
[17] E. Kask, T. Raadik, M. Grossberg, R. Josepson, *Energy Proc.* **2011**, *10*, 261.
[18] O. Gunawan, T. Gokmen, C. W. Warren, J. D. Cohen, K. Teodor, D. A. R. Barkhouse, S. Bag, J. Tang, B. Shin, D. B. Mitzi, *Appl. Phys. Lett.* **2012**, *100*, 253805.
[19] A. Jasenek, U. Rau, V. Nadenau, H. W. Schock, *J. Appl. Phys.* **2000**, *87*, 594.
[20] T. Walter, R. Herberholz, C. Muller, H. W. Schock, *J. Appl. Phys.* **1996**, *80*, 4411.
[21] J. T. Heath, J. D. Cohen, W. N. Shafarman, *J. Appl. Phys.* **2004**, *95*, 1000.
[22] B. Lei, W. W. Hou, S.-H. Li, W. Yang, C.-H. Chung, Y. Yang, *Sol. Energy Mater. Sol. Cells* **2011**, *95*, 2384.
[23] D. B. Mitzi, O. Gunawan, T. K. Todorov, K. Wang, S. Guha, *Sol. Energy Mater. Sol. Cells* **2011**, *95*, 1421.
[24] S. S. Hegedus, W. N. Shafarman, *Prog. Photovoltaics* **2004**, *12*, 155.
[25] O. Gunawan, T. K. Todorov, D. B. Mitzi, *Appl. Phys. Lett.* **2010**, *97*, 233506.
[26] L. C. Kimerling, *J. Appl. Phys.* **1974**, *45*, 1839.
[27] J. Lee, J. D. Cohen, W. N. Shafarman, *Thin Solid Films* **2005**, *480–481*, 336.
[28] R. Haight, A. Barkhouse, O. Gunawan, B. Shin, M. Copel, M. Hopstaken, D. B. Mitzi, *Appl. Phys. Lett.* **2011**, *98*, 253502.
[29] R. Herberholz, M. Igalson, H. W. Schock, *J. Appl. Phys.* **1998**, *83*, 318.
[30] Q. Cao, O. Gunawan, M. Copel, K. B. Reuter, S. J. Chey, V. R. Deline, D. B. Mitzi, *Adv. Energy Mater.* **2011**, *1*, 845.
[31] J. Heath, J. Cohen, W. N. Shafarman, *Thin Solid Films* **2003**, *432*, 426.
[32] T. Eisenbarth, T. Unold, R. Caballero, C. A. Kaufmann, H.-W. Schock, *J. Appl. Phys.* **2010**, *107*, 034509.
[33] M. Turcu, U. Rau, *Thin Solid Films* **2003**, *432*, 158.
[34] D. Cahen, R. Noufi, *Appl. Phys. Lett.* **1989**, *54*, 558.
[35] J. Vidal, S. Botti, P. Olsson, J.-F. Guillemoles, L. Reining, *Phys. Rev. Lett.* **2010**, *104,* 056401.
[36] M. J. Romero, H. Du, G. Teeter, Y. Yan, M. M. Al-Jassim, *Phys. Rev. B* **2011**, *84*, 165324.
[37] E. Zscherpel, J. Scragg, S. Siebentritt, *Physica B* **2009**, *404*, 4949–4952.
[38] F. Luckert, D. I. Hamilton, M. V. Yakushev, N. S. Beattie, G. Zoppi, M. Moynihan, I. Forbes, A. V. Karotki, A. V. Mudryi, M. Grossberg, J. Krustok, R. W. Martin, *Appl. Phys. Lett.* **2011**, *99*, 062104.
[39] J. P. Leitao, N. M. Santos, P. A. Fernandes, P. M. Salome, A. F. Cunha, J. C. Gonzalez, G. M. Ribeiro, F. M. Matinaga, *Phys. Rev. B* **2011**, *84,* 024120.
[40] H. Zhao, C. Persson, *Thin Solid Films* **2011**, *519*, 7508–7512.
[41] S. Lany, A. Zunger, *Phys. Rev. B* **2005**, *72*, 035215.
[42] M. Igalson, P. Zabierowski, D. Prządo, A. Urbaniak, M. Edoff, W. N. Shafarman, *Sol. Energy Mater. Sol. Cells* **2009**, *93*, 1290.
[43] G. Hanna, A. Jasenek, U. Rau, H. W. Schock, *Phys Status Solidi A* **2000**, *179*, R7.
[44] V. Nadenau, U. Rau, A. Jasenek, H. W. Schock, *J. Appl. Phys.* **2000**, *87*, 584.
[45] I. L. Repins, B. J. Stanbery, D. L. Young, S. S. Li, W. K. Metzger, C. L. Perkins, W. N. Shafarman, M. E. Beck, L. Chen, V. K. Kapur, D. Tarrant, M. D. Gonzalez, D. G. Jensen, T. J. Anderson, X. Wang, L. L. Kerr, B. Keyes, S. Asher, A. Delahoy, B. Von Roedern, *Prog. Photovoltaics* **2006**, *14*, 25.
[46] W. W. Hou, B. Bob, S. Li, Y. Yang, *Thin Solid Films* **2009**, *517*, 6853.
[47] D. B. Mitzi, L. L. Kosbar, C. E. Murray, M. Copel, A. Afzali, *Nature* **2004**, *428*, 299.